

## An application of the multibeam sounder for seabed backscattering analysis

BISHWAJIT CHAKRABORTY and Y. SATYANARAYANA RAJU  
National Institute of Oceanography,  
Dona Paula, Goa : 403004

*A theoretical analysis of vertical farfield pattern for a multibeam sounder is performed. The farfield pattern for different steered angles establish the usefulness of present multibeam arrays. An interaction effect of different steered multibeam signals are studied with the sediments like sand, clay and silt of smooth and rippled type. Study shows that the scattering effect is less with the sand bottom while compared with clay and silt type sediments.*

### Introduction

Sonar reflection profiling of the seafloor is a routine method for various objectives, such as geological surveys to characterize the seabed, geotechnical properties, and resource evaluation of polymetallic nodules. Single narrow beam sounders were long being used for some of the above purposes. But significant improvement in swath sounding system resulted in multibeam sounders replacing single beam equipment. Multibeam is also found to be effective from the economic point of view of maintaining the high accuracy and applicability even in rough sea condition<sup>1-2</sup>. Being a high resolution system, multibeam sounders transmit/receive narrow beams along with suppressed side lobes. The steering of beams are performed using appropriate delays across the elements. The present communication deals with the mathematical formulation and theoretical analysis of a multibeam sounder of sixty elements. The vertical farfield patterns of different steered directions are also presented.

In order to classify the seabed, the interaction effect of the bottom relief on an acoustical signal

must be known. Stanton and Clay, Dunsiger *et. al.*, and many workers have carried out work to identify the bottom type from its reflection and scattering characteristics<sup>3-5</sup>. Multibeam sounder system has the potential to provide a quantitative backscattered information which is useful to classify the seabed<sup>6</sup>. But the complexity of seabed geomorphology prevents single empirical formulation of the scattered signal from experimental observations. Tjotta and Tjotta<sup>5</sup> developed a theory for the reflected and refracted signal from the sea bottom. Their theory was found to be in good agreement with Muir *et. al.*'s experiments<sup>7</sup>. In this study we have used Tjotta and Tjotta's theory for a computation of the backscattering coefficients of seabeds like sand, clay and silt sediment types. The rippled bottom parameters of above are given by Chakraborty<sup>8</sup>.

Stanton demonstrated that the Probability Density Function (PDF) of echo amplitude depends on the seafloor roughness, sonar beamwidth and frequency, especially at low frequency where the wavelength of the sound signal is much greater than the root mean square (rms) roughness of the seafloor<sup>9</sup>. Based upon the Stanton's work PDF's are

**Table 1. Properties of the rippled bed**

Sediment type	rms ripple roughness (m)	Correlation ripple wavenumber (m <sup>-1</sup> )		Density (g/cc.)	Sound Velocity (m/s)
		along x-axis	along y-axis		
Sand	0.011	14.69	2.94	2.03	1836
Clay	0.013	11.92	2.38	1.42	1519
Silt	0.015	9.98	1.99	1.56	1522

calculated for different rippled bottom (Table 1) for the centre beam.

**Theoretical Analysis**

Fig. 1 shows a linear array kept on XY-plane. The array of the multibeam sonar consists of 60 elements and they are kept along x-axis. The array is centred at the origin of the coordinate, and symmetrical about z-axis. The separation between array elements are considered to be 0.3 λ where λ is the design wavelength.

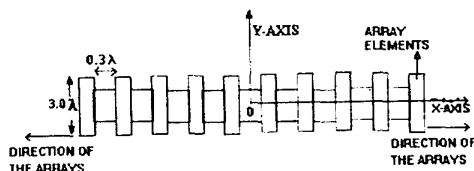


Fig. 1 Multibeam array geometry

**Farfield Pattern :**

The farfield radiation pattern for a linear array is given by<sup>10</sup>

$$[F(\theta, \phi)] = [f(\theta, \phi)]. [Element Pattern]. \dots\dots (1)$$

The array factor  $f(\theta, \phi)$  is given by

$$f(\theta, \phi) = \sum_{m=1}^M A_m \exp(j \cdot \vec{k} \cdot \vec{r}_m \cdot \vec{R}). \dots\dots (2)$$

$A_m$ , the complex excitation coefficient, is assumed to be unity and  $k=2\pi/\lambda$ .  $M$  is the number of elements within the array and is equivalent to 60 for our study. The operating frequency is assumed to be 15 kHz. In eqn. (2),

$$\vec{r}_m = d_m \vec{i}, \dots\dots (3)$$

$d_m$  is the interelement separation and  $\vec{i}$  is unit vector along x-axis. The vector  $\vec{R}$  can be rewritten as

$$\vec{R} = c \sin \theta \cos \phi \vec{i} \dots\dots\dots (4)$$

So the array factor for linear array can be given by

$$f(\theta, \phi) = \sum_{m=1}^{60} \exp j k (d_m \sin \theta \cos \phi) \dots\dots (5)$$

The phase delay require across the elements for steering the beam along the direction  $\theta, \phi$ , expressed as

$$\alpha_m = -d_m k (\sin \theta_0 \cos \phi_0) \vec{i} \dots\dots\dots (6)$$

The above phase term when used in eqn (5) the array factor is given by

$$f(\theta, \phi) = \sum_{m=1}^{60} \exp j k (d_m \sin \theta \cos \phi - d_m \sin \theta_0 \cos \phi_0) \dots\dots\dots (7)$$

In eqn. (1), the element pattern is rewritten as

$$Element Pattern = \frac{\sin(\pi l \sin \theta \sin \phi)}{(\pi l \sin \theta \sin \phi)} \dots\dots (8)$$

Where  $l$  is the length of the element and is equivalent to  $3.0 \lambda$ . The width of the elements are negligible compared to it's length. Final expression for the vertical farfield pattern can be obtained by substituting eqn's (7) and (8) in eqn. (1).

Farfield pattern for multibeam array of above type is shown in Fig. 2. The half power beamwidths are slowly increasing ( $2.7^\circ, 2.8^\circ, 2.9^\circ$  and  $3.2^\circ$ ) at  $0^\circ, 10^\circ, 20^\circ$  and  $30^\circ$  angles respectively. The beamwidths are narrow, hence useful for high resolution applications. The maximum sidelobe level of -13 dB is obtained for incidence angles of  $30^\circ$ . Apart from above incidence angles (Fig. 2), there are other angles  $5^\circ, 15^\circ, 25^\circ$  and computed half power beamwidths at these angles are  $2.7^\circ, 2.8^\circ$  and  $3.0^\circ$  respectively. In later part of the present work these information of

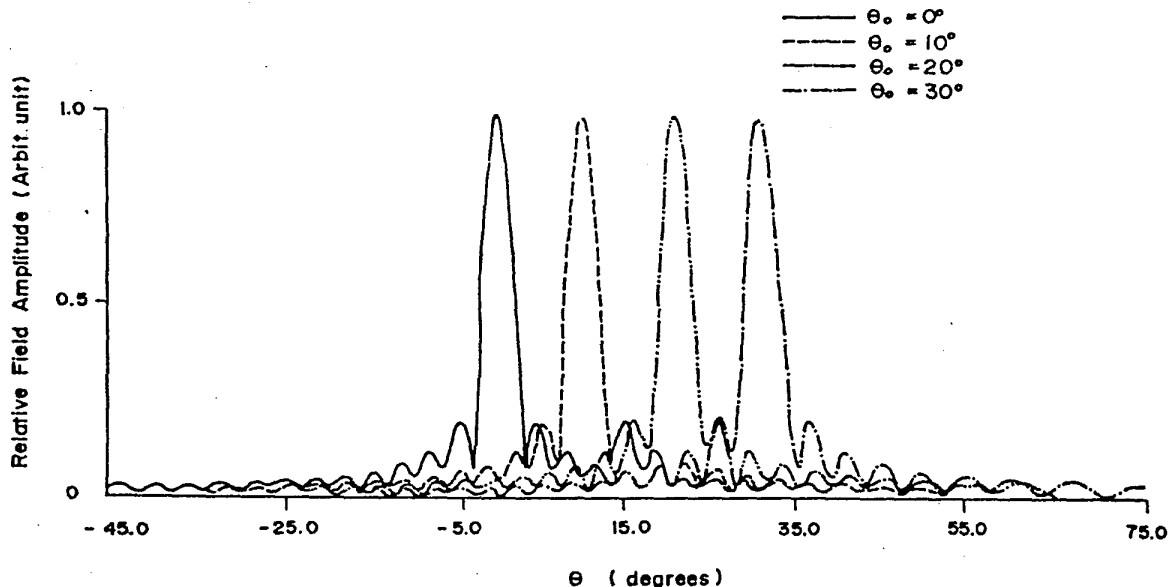


Fig. 2 Beampattern of the array for  $\phi=0^\circ$  -plane

half power beamwidths are used for backscattering calculations.

**Backscatter Analysis**

We assume that array is hull mounted and water depth is 5000m. The spot produced by the beam acts as a sound source which is reflected from the sediment. The present study is carried out for the echoes reflected back from water / seabed interface i.e., penetration effects are not considered. The scattered pressure at a farfield from the spot may be expressed by<sup>5</sup>

$$P_o(r, \theta', \phi) = R_o \frac{jks}{2\pi r \cos\theta} p \exp(i k r) \bar{F}(\theta', \phi) \quad \dots\dots\dots (9)$$

The above expression is obtained based on the idea that the amplitude of the incident beam ( $p$ ) is constant within the spot area (assumed to be unity in the present case) and zero elsewhere.  $r, \theta', \phi$  are the spherical coordinates measured from the spot.  $r$  is the distance from the spot to the point of observations i.e., range. For reflection from the bottom towards the same direction of the angle of incidence  $\theta = -\theta'$ .  $s$  is the area of the spot. Fig. 3 illustrates detail operating conditions. The term  $\bar{F}(\theta', \phi)$  is given as

$$F(\theta', \phi) = \cos \theta' (\sin \epsilon_x / \epsilon_x) (\sin \epsilon_y / \epsilon_y) \dots\dots\dots (10)$$

$$\text{where } \epsilon_x = (a_x / \cos \theta) (k \sin \theta' \cos \phi - k \sin \theta) \dots\dots\dots (11)$$

$$\text{and } \epsilon_y = a_y k \sin \theta' \sin \phi. \dots\dots\dots (12)$$

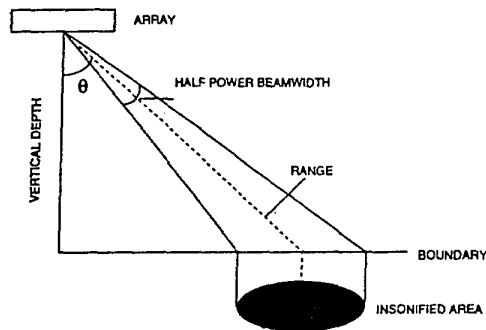


Fig. 3 Geometry of the problem

$a_x$  is the half of the half power beamwidth (HPBW) along x-axis. The HPBW along x-axis is already computed using eqn. (1). And,  $a_y$  is half of the HPBW along y-axis i.e., along ship's direction which is assumed to be  $3.1^\circ$ .

The reflection coefficient,  $R_o$  is written as<sup>11</sup>

$$R_o = \frac{m \cos \theta - (n^2 - \sin^2 \theta)^{0.5}}{m \cos \theta + (n^2 - \sin^2 \theta)^{0.5}} \quad \dots\dots\dots (13)$$

m is  $\phi_1 / \phi$ ,  $\phi_1$  is the density of the sediments and  $\phi$  is density of the seawater. n is  $c/c_1$ , c and  $c_1$  are the sound velocities of the water and sediments. In this study, density and sound velocity of the sea water is assumed to be 1.03 g/cm<sup>3</sup> and 1500 m/sec. respectively. The values of the sediment sound velocity and density are given in Table 1. The reflected signal is known to be the signal from the smooth bottom of different sediments over the seabed. In order to know the scattered signal from the rippled bottom of different sediment types, the mean scattered signal may be expressed<sup>12</sup>

$$\langle p \rangle = P_0 \exp^{-2\gamma^2 \Omega^2} \dots \dots \dots (14)$$

For our case,  $\gamma$  the vertical component of the reflected and incident wavenumber is equal to  $-k \cos \theta'$ ,  $\Omega$  is the rms ripple height (Table 1.) and  $P_0$  is reflected pressure from mirror like bottom of respective sediment type.

In logarithmic scale backscattering strength is a scattering coefficient  $n'$

$$M = 10 \log n' \dots \dots \dots (15)$$

and  $n'$  may be written as

$$n' = p'^2 \dots \dots \dots (16)$$

$p'$  is a pressure wave reflected from smooth or rippled bottom of different sediment type at particular incident angle. Hence for smooth bottom  $p'$  is equivalent to  $P_0$  and for rippled bottom it is equal to  $\langle p \rangle$ .

Fig. (4) shows plot between the backscattering strength (dB) with incidence angles varying from 5° to 30°, a clear look on the figure ensures that the backscattering strength for smooth sandy bottom is the highest while compared with other bottoms of smooth and rippled type. Again, the backscattering strength is maximum for the angle at 5° and slowly decreases up to 30°. On the whole it can be concluded that the level of backscattering pattern changes for sediments of sand, clay and silt of rippled and smooth type, but their shape remain unchanged. The back-scattering strength values presented here up to near normal incidence angle of 25° is comparable with the experimental results of Urick<sup>13</sup>, and Brekhovskikh and Lysanov<sup>11</sup> for deeper water at abyssal plain. Another important factor which is clearly observed in our study is the dependence of the

backscatter level with the characteristics / nature of the water bottom boundary (dependence of backscatter level on sediment types). We find a significant changes in the scattering strength. This fact is similar with the concept drawn by Brekhovskikh *et al*<sup>14</sup>.

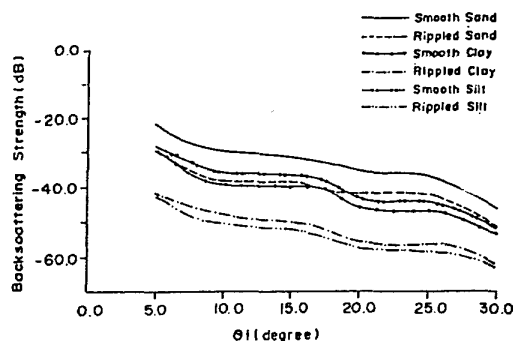


Fig. 4 Backscattering strength with respect to the angle of incidence

### Echo Fluctuation

In order to know the fluctuation of echoes from rippled seabottoms like sand, clay and silty types, a study is undertaken for computation of the PDF of the echoes measured from center beam of the array.

The Rice PDF may be expressed for echo amplitude from seabed<sup>9</sup>

$$P(e) = [2e (1+g)/\langle e^2 \rangle] \exp \{-(1+g) e^2 + g \langle e^2 \rangle\} I_0(q) \dots \dots \dots (16)$$

where  $I_0(q)$  is the modified Bessel function and

$$q = 2 e [g (1 + g)]^{0.5} / (\langle e^2 \rangle) \dots \dots \dots (17)$$

$\langle e^2 \rangle$  is the mean square echo amplitude and  $g$  is the measure of the relative roughness or smoothness of the bottom. It can be presented as

$$g^{-1} = (300 / \pi) b^2 k^4 \Omega^{4.5} \eta \dots \dots \dots (18)$$

$b$  is the full power beamwidth in radians of the multibeam sounder, and is 4.25° in present study. For PDF calculations the full power beamwidths along x and y axes are nearly same for normal incidence direction.  $\eta$  term is varying from 1-5. In the present study,  $\eta$  is chosen to be 5 i.e., the variation of ripple waves along y axis is 5 times to the variation along x axis.

Fig. 5 shows the narrowest PDF which is obtained for sandy rippled bottom. Similarly the PDF's are broader for clay and silt because of their higher rms roughness. The PDF is Gaussian type for sand ripple and roughness is increasing for clay and silt ripples. Again, the above fact is supported by computed values of  $g^{-1}$ , which is presented in Fig. 5.

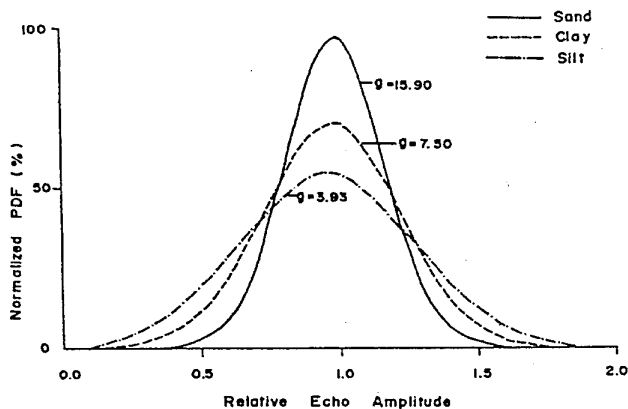


Fig. 5 PDF for different rippled sediment types

## Conclusion

The expression for the farfield pattern of a multibeam sounder is developed. The narrow main beam width with less sidelobe level confirm the suitability of such an array for multibeam use. Echo fluctuation for centre beam and computed backscattering strength for outer beams show that the backscattering strength is highest for sandy bottoms and is less for clay and silty bottom. Backscattering strength decrease with the angle of incidence for all the sediment type but no change of the shape of the scattered pattern is observed with the bottom type.

## References

1. de Moustier, C., State of the art in swath bathymetric survey system, *Int. Hydro. Review (USA)*, **65** (1988) 25-34.
2. Jantti, T. P., Trials and Experimental results of the Echoes XD Multibeam Echosounder, *IEEE J. Ocean Eng.*, **14**, (1989) 306-313.
3. Stanton, T. K. and Clay, C. S., Sonar Echo Statistics as a remote sensing tool, *IEEE J. Ocean Eng.*, **11** (1986) 79-90.
4. Dunsiger, A. D., Cocharane, N. A. and Vettor, N. J., Seabed characterization from broadband acoustic echosounding with scattering models, *IEEE J. Ocean Eng.* **6** (1981) 94-107.
5. Tjotta, J. N., and Tjotta, S., Theoretical study of penetration of highly directional acoustics Beam, *J. Acoust. Soc. Am.*, **85** (1981) 998-1008.
6. de Moustier, C., Beyond Bathymetry : Mapping acoustic backscattering from deep seafloor with Seabeam, *J. Acoust. Soc. Am.*, **79** (1986) 316-331.
7. Muir, T. G., Horton, Sr., C. W., and Thompson, L. A., The penetration of highly directional beams into the sediments, *J. Sound and Vibration*, **64** (1971) 538-551.
8. Chakraborty, B., Effects of scattering due to seafloor microroughness on a multifrequency sonar seabed profiler, *J. Acoust. Soc. Am.*, **85** (1989) 1478-1481.
9. Stanton, T. K., Sonar estimates of the seafloor microroughness, *J. Acoust. Soc. Am.*, **75** (1984) 809-818.
10. Collins, R. F., and Zucker, F. J., *Antenna Theory*, Mc Graw Hill, New York (1969).
11. Brekhovskikh, T., and Lysanov, Y., *Fundamental of Acoustics*, Springer Verlag, Berlin (1982).
12. Tolstoy, I., and Clay, C.S., *Ocean Acoustics : Theory and Experiments in Underwater Sound*, Mc Graw Hill, New York (1966).
13. Urick, R. J., *Principles of Underwater Sound* Mcgraw Hill, Singapore (1975)
14. Brekhovskikh, T., Zhitkovskikh, Y. Y., Zakhlestein, A. Y., and Savelev, V. V., Sound scattering by ferromanganese concretion, *Sov. Phys. Acoust.*, **31** (1985) 343-344.